Slow tail of nematic spin fluctuations in $Ba(Fe_{1-x}Co_x)_2As_2$: Insight from nuclear magnetic resonance

Jaafar N. Ansari,[1,*] Karen L. Sauer,[1,2,†] and Igor I. Mazin[1,2,‡]
[1]*Department of Physics and Astronomy, George Mason University, Fairfax, Virginia 22030, USA*
[2]*Quantum Science and Engineering Center, George Mason University, Fairfax, Virginia 22030, USA*

(Received 2 February 2023; revised 20 June 2023; accepted 4 August 2023; published 25 August 2023)

The two most interesting properties of Fe-based superconductors (FeSCs), high-temperature superconductivity and nematicity, are widely believed to come from spin fluctuations (SF). One of the least studied aspects of SF are their frequency spectrum, albeit it is generally believed that SF in FeSCs can be roughly separated into (1) fast SF in the spin space which preserve the local nematic correlations, (2) slow SF in the real space, where the sense of the local nematic order fluctuates, and (3) the high-energy SF which break the local nematic order. Although, the latter are probably irrelevant in the entire observable temperature range. Nuclear quadrupolar interactions, as opposed to magnetic interactions, are sensitive only to SF in the real space, and only to those slower than its characteristic timescale. We combine existing nuclear magnetic resonance data on electric field gradient anisotropy with first-principles calculations to access the amplitude of the real-space (nematic) SF on the timescale *above* the actual nematic transition in $BaFe_2As_2$ as a function of Co doping. This demonstrates exceptionally slow dynamics of nematic fluctuations even in the formally tetragonal phase.

DOI: 10.1103/PhysRevB.108.064516

I. INTRODUCTION

Spin fluctuations (SF) in Fe-based superconductors (FeSCs) are generally believed to be essential for the two most intriguing phenomena in this family of materials: High-temperature superconductivity [1,2] and nematic order [3,4]. At least in the latter case, the effect of SF is intimately connected to the quasi-two-dimensional (quasi-2D) character of FeSCs, whereby the magnetic order (observed in most, albeit not all, FeSC parent compounds) is destroyed by slow, long-range SF stemming from the nearly rotational invariance of the Heisenberg Hamiltonian, known as the Mermin-Wagner theorem [5]. Theoretical or Monte Carlo treatment of Mermin-Wagner physics is challenging, and little is known quantitatively about the spectrum of such fluctuations in FeSCs. Hence, developing a quantitative picture of SF is a critical piece in the puzzle of better understanding such unconventional superconductors.

One can discuss two types of SF in such isotropic spin systems, which can be conditionally called real-space and spin-space fluctuations. Shown in Fig. 1, spin-space fluctuations maintain, at any moment of time, the local collinear "stripe" orientation, breaking the local C_4 symmetry in an Fe plaquette, and keeping the same "sense" of the stripe orientation. That is, spins can point in any direction, but remain collinear and parallel along one crystallographic direction (e.g., a) and antiparallel along the other (b). On the other hand, real-space fluctuations are fluctuations between two different local stripe orientations. It has been shown [3,6] that real-space fluctuations freeze first, creating the so-called nematic state and thus breaking statically the global C_4 symmetry. Spin-space fluctuations are not frozen out in the nematic phase, but freeze at some lower temperature.

In principle, at very high temperatures one can imagine SF that break the local stripe order, generating transient ferromagnetic, ferrimagnetic, or checkerboard-antiferromagnetic configurations. However, the anisotropy of the high-temperature nuclear magnetic resonance (NMR) relaxation rates convincingly shows that such temperatures are not attainable in real experiments [7,8]. Detecting either fluctuation will of course depend on the timescale of the experimental probe. When the timescale of a probe is greater than the fluctuations' timescale, and/or its length scale is much longer than the fluctuations', the fluctuations will be completely averaged out and undetectable. This is the case, for instance, in neutron scattering, where a lower-ordered Fe moment, relative to fast local probes, is measured [9]. However, it is generally believed that even close above the nematic transition, real-space fluctuations are sufficiently fast to not generate any observable local C_4 symmetry breaking. This belief, however, is in conflict with two recent observations [10,11] that detected via NMR a nonzero C_2 anisotropy of electric field gradients (EFG) in FeSCs well above the Neel transition. This suggests that a measurable fraction of SF is slower than the NMR timescale, typically on the order of microseconds [12]. Beyond NMR, a very similar concept, dubbed "nematic liquid", has been introduced in $BaNi_2As_2$ to explain a phonon-line splitting incompatible with the tetragonal symmetry [13].

In this paper, we *quantify* this result, establishing a direct link between the observed EFG asymmetry and the average amplitude of those real-space fluctuations that are *slower*

*jansari@gmu.edu
†ksauer1@gmu.edu
‡imazin2@gmu.edu

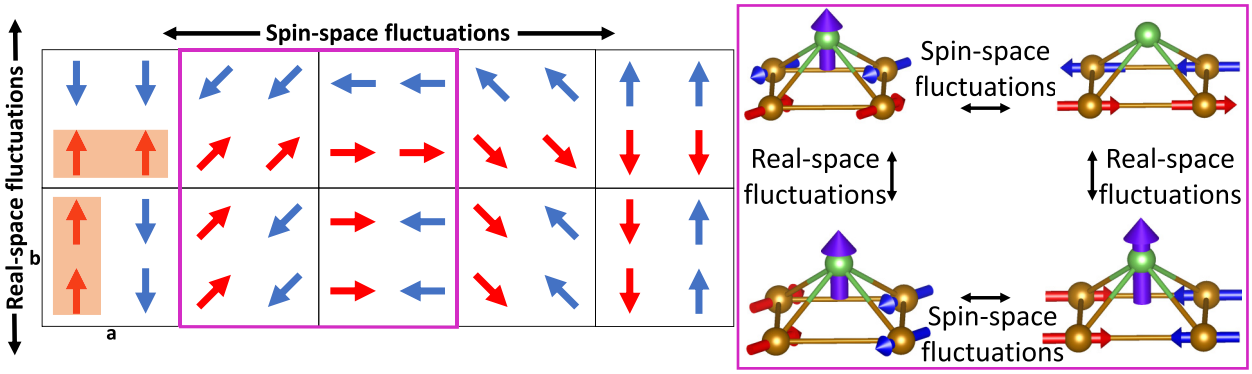

FIG. 1. Visualization of real-space and spin-space fluctuations of the Fe magnetic moments (red and blue arrows) in connected Fe plaquettes. Four plaquettes are highlighted in the magenta boxes, showing a mapping between the 2D and 3D representations of the unit cell and the corresponding fluctuations. The 3D view contains the As site and the resulting hyperfine field it experiences as a purple arrow. Real-space fluctuations are fluctuations of the stripe direction, indicated by the orange box. Spin-space fluctuations are continuous, long-range-order fluctuations such that Fe moments may point in any arbitrary direction while maintaining collinearity.

than the NMR timescale. To this end, we use first-principles density functional theory (DFT) with tunable Hund's Stoner coupling, also known as Hund's rule coupling [14].

II. BACKGROUND OF NUCLEAR MAGNETIC RESONANCE

In the case of Fe-based superconductors, many compounds have nuclei with spin $I = \frac{3}{2}$ situated at the center above the Fe plane. This nucleus will experience energy level splitting due to any external magnetic field, the hyperfine field generated by the Fe magnetic moments, and the interaction of its electric quadrupole moment with the local electronic environment. Therefore, the full nuclear Hamiltonian is given by the combination of the Zeeman and electric quadrupolar Hamiltonians [15]:

$$H = -\gamma\hbar\mathbf{H}_{\text{eff}}\cdot\mathbf{I} + \frac{eQ}{4I(2I-1)} \times \left[V_{zz}\left(3I_z^2 - I^2\right) + (V_{xx} - V_{yy})\left(I_x^2 - I_y^2\right)\right], \quad (1)$$

where γ is the gyromagnetic ratio of the nucleus, $\mathbf{I}$ is the spin angular momentum operator, and $\hbar$ is the reduced Planck's constant. The total magnetic field felt by the nucleus is $\mathbf{H}_{\text{eff}}$ and Q is its electric quadrupole moment. The V_{ij} are the components of the electric field gradient (EFG) tensor and are the main quantities used to describe the electric interaction. They are defined by $V_{ij} = \partial^2 V/\partial x_i \partial x_j|_{\mathbf{r}=\mathbf{r}_0}$, where V is the electrostatic potential, x_i are real-space coordinates, and $\mathbf{r}_0$ is the position of the nucleus. An additional parameter, known as the EFG asymmetry parameter, is commonly defined as $\eta = (V_{xx} - V_{yy})/V_{zz}$, where it is convention to define the axes such that $|V_{zz}| \geqslant |V_{yy}| \geqslant |V_{xx}|$ so as to restrict η to be less than unity. Now Eq. (1), as written, assumes a principal axes frame, that is, $V_{ij} = 0$ for $i \neq j$. At a crystallographic site of full orthorhombic symmetry, as, for instance, in this case, the principal axes frame coincides with the crystallographic axes, and, apart from an accidental cancellation, symmetry dictates that $\eta \neq 0$.

The exact diagonalization of Eq. (1) is available in the literature [16]. In the case of NMR with a large external magnetic field, the quadrupolar interaction is a perturbation on the Zeeman effect. We utilize the usual convention of defining the crystallographic axes as follows: a axis aligned with the antiferromagnetic direction, b axis aligned with the ferromagnetic direction, and c axis perpendicular to the Fe plane. Adopting θ and φ to be the polar and azimuthal angles of $\mathbf{H}_{\text{eff}}$ with respect to the c axis, second-order perturbation theory gives the dominant transition frequencies as [7,17]

$$\nu_{m\leftrightarrow m-1} = \frac{\gamma H_{\text{eff}}}{2\pi} + \frac{eQV_{cc}}{4h}\left(m - \frac{1}{2}\right) \times \left(3\cos^2\theta - 1 + \frac{V_{aa} - V_{bb}}{V_{cc}}\sin^2\theta\cos 2\varphi\right), \quad (2)$$

for $m = \frac{3}{2}, \frac{1}{2}, -\frac{1}{2}$. In the case that there is no static magnetic field on the nucleus, the Hamiltonian reduces to just the second term of Eq. (1). This type of NMR, called zero-field NMR or nuclear quadrupole resonance (NQR), has a twofold degeneracy for spin-$\frac{3}{2}$ systems and thus has only one transition frequency [18]:

$$\nu_Q = \frac{eQV_{cc}}{2h}\sqrt{1 + \frac{1}{3}\left(\frac{V_{aa} - V_{bb}}{V_{cc}}\right)^2} \quad (3)$$

$$= \frac{eQ}{\sqrt{6}h}\sqrt{V_{aa}^2 + V_{bb}^2 + V_{cc}^2}, \quad (4)$$

where the final equality can be achieved by invoking Laplace's equation $V_{aa} + V_{bb} + V_{cc} = 0$, which is justified since spherically symmetric charge densities found at the nucleus do not affect the transition frequencies [15]. Thus, to determine the full EFG from only the transition frequencies, only NMR, and not zero-field NMR, can be used.

From this point forward, it is useful to depart from the conventional definition of η and alternatively use

$$\eta = \frac{V_{aa} - V_{bb}}{V_{cc}}. \quad (5)$$

It is not necessarily always the case that the magnitude of V_{cc} is the largest of the three components, hence, η defined in this way is unrestricted in its range of values.

III. EXISTING EXPERIMENTAL DATA AND PREVIOUS INTERPRETATION

Since the discovery of FeSCs, NMR has been a fruitful tool in understanding the phase diagram and the superconducting state of a variety of FeSCs [19–21]. Two groups have directly performed measurements that address the anisotropy of the Fe plane manifested by η: (1) in the paramagnetic phase in $Ba(Fe_{1-x}Co_x)_2As_2$ [10,11] and (2) in doped 111 materials [11,22]. The primary focus of this study is the results of the former while the latter systems will be addressed in a future publication.

It is worth mentioning that other groups have also used η as a primary quantity for investigation. For instance, undoped $BaFe_2As_2$ was studied in Ref. [7] and $SrFe_2As_2$ in Ref. [23], but these studies did not perform measurements in the paramagnetic phase. On the other hand, EFGs were used to study the nematic susceptibility in the paramagnetic phase of strained $BaFe_2As_2$ [24].

In Ref. [10], experiments on single-crystal $Ba(Fe_{1-x}Co_x)_2As_2$ for $x = 0, 0.02, 0.05, 0.08$ using ^{75}As NMR in the paramagnetic phase were reported. Due to the Co doping, there are several distinct As positions. Adopting their notation, "As0" is the site with no Co atoms among either the nearest- or the next-nearest-neighbor Fe sites. "As0n" refers to the site with zero Co atoms among the nearest-neighbor Fe sites and n Co atoms at the next-nearest-neighbor Fe sites. "As1" sites, correspondingly, have a Co atom in the nearest-neighbor shell. For the purposes of this paper, only the results from As0 measurements are addressed and the other As sites are only briefly commented on later in this section. For each concentration, small but nonzero η were measured, indicating C_4 symmetry breaking of the Fe plane. While the authors have positively excluded any external strain, for instance from gluing the sample to the holder, they suggested [10,11] that the nonzero η originates from internal strain coming from unspecified native defects or induced by a long-range effect of Co impurities. Next, this interpretation is discussed in detail before an alternate explanation is offered.

Specifically, they noticed that η varies with temperature according to the Curie-Weiss law $C_W/(T - T_\eta)$. It was also observed that the dependence of T_η on the Co concentration is relatively similar to that of the Curie-Weiss temperature T_χ determined, for instance, from the temperature dependence of the nematic susceptibilty χ_n extracted from the Raman response under no external stress. The quantity χ_n is defined to be the degree of deviation of the electronic properties from the C_4 symmetry induced by an in-plane unit strain. If one defines a measurable C_2 quantity as S (for instance, the component of the Raman tensor that is forbidden under the C_4 symmetry), then $S = \chi_S\sigma$, where σ is the strain. In the linear response regime, selecting a different S would only change the overall scaling of χ_S. In addition, the antiferromagnetic Curie-Weiss temperature T_m, deduced from the $1/TT_1$ relaxation rate, behaves similarly to T_χ as a function of temperature, but remains always higher.

The authors of Ref. [11] argue then that existing defects and impurities generate random local temperature-independent strains. Adding more Co increases the concentration of the impurities and the relative volume of the sample affected by the strain. Then, an As ion that finds itself in a locally strained region, say near a Co impurity, experiences an asymmetric EFG, proportional to $\chi_n(T)$. This interpretation has two appealing characteristics: (1) it explains the similarity between T_η and T_χ and (2) it is qualitatively consistent with the rapid increase of the Curie-Weiss numerator C_W with Co doping.

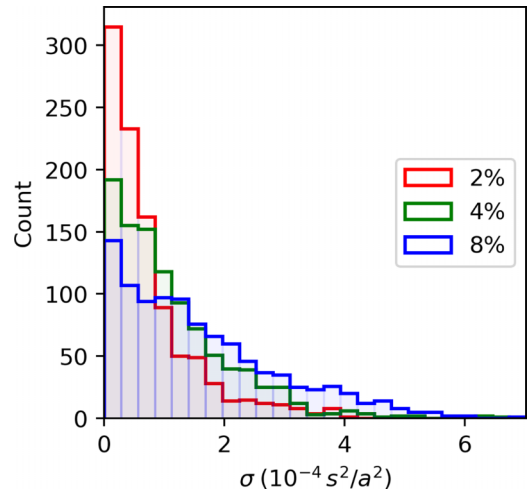

FIG. 2. Monte Carlo simulation of local strain due to Co impurities in a supercell for different Co concentrations. The strain decays as $1/r^2$, which is the most reasonable decay rate for this situation. Here, s is a characteristic length and the results are normalized with respect to the a lattice parameter. The distributions are broad enough that many different η values would exist, making an NMR measurement of η difficult.

On the other hand, there are some unclarified aspects in this interpretation. The strain generated around an impurity is isotropic and rapidly decaying, so one would expect different As sites to experience a broad distribution of strains and therefore η values.

A simulation of the effects of impurities is now presented to support the above claims. In order to emulate the effect of random point defects, in this case Co impurities, on the local strain distribution in 2D media, a large number of randomly distributed defects were generated in a 1001×1001 supercell, using concentrations of 2%, 4%, and 8%. The nematic strain at the central point is then calculated using $\sigma = |\varepsilon_{xx} - \varepsilon_{yy}|$, where the strain tensor is given by $\varepsilon_{ij} \sim s^2 r_i r_j / r^4$ and s is a characteristic length. Assuming a simple elastic media, this strain tensor is calculated using the displacement vector $u \sim 1/r$ derived in Sec. 7, Problem 4 of Ref. [25], but excluding the isotropic term which does not couple to the nematic order parameter. Calculating the strain in this way captures the nematic susceptibility and gives a $1/r^2$ strain decay rate. This is the most reasonable decay rate to use for this simulation, though it is noted that it can even be exponential [26]. To collect enough statistics, this process was repeated 1000 times, excluding rare cases when the central point had one nearest or next-nearest defect neighbor.

The results are presented in Fig. 2. A few observations can be made. First, because of strong cancellation of the strains coming from different impurities, the magnitude of the average strain is four orders of magnitude smaller than the strain

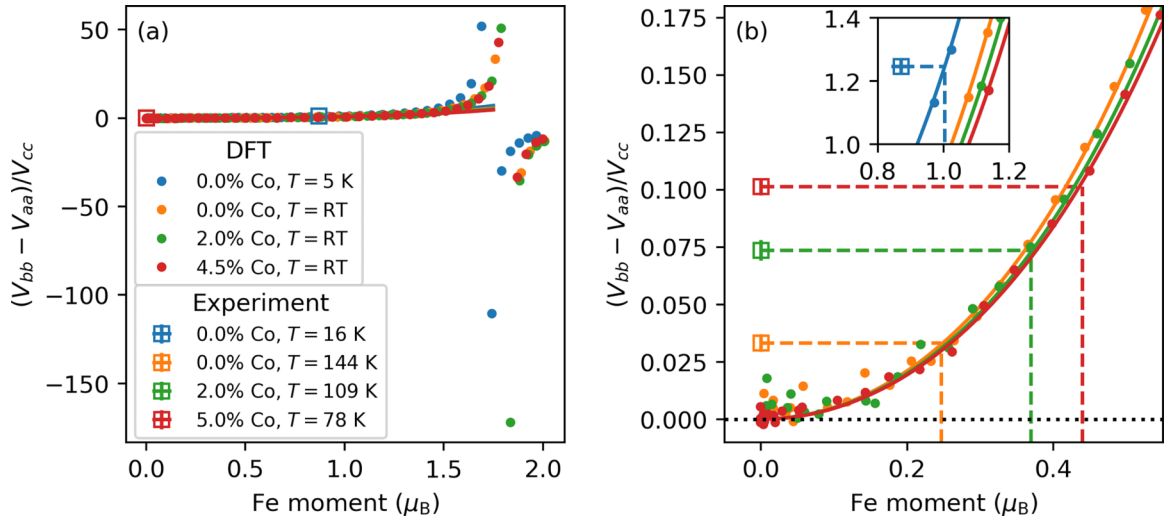

FIG. 3. DFT calculations of the electric field gradient asymmetry parameter as a function of the Fe magnetic moment per Fe site, with (a) the full results and (b) a zoomed-in view showing the experimental data points for comparison. The largest Fe moment value corresponds to the value given by DFT without any scaling down of the spin-dependent part of the exchange and correlation functional. The nonzero experimental asymmetry values can be used to extract an effective magnetic moment as probed by NMR, indicated by the intersecting dashed lines. The experimental data were pulled from literature [7,10] in both the orthorhombic and paramagnetic phases. The DFT calculations used experimental lattice parameters [29,30] as inputs. The temperatures at which the lattice parameters were determined are indicated in the legend.

induced by an isolated impurity upon its nearest-neighbor sites, and at least two orders of magnitude smaller than what is observed in the experiments. Note that the number of nearest neighbors increases with concentration, but the number of sites far away (As00) is roughly the same as long as the concentration is small. Additionally, while the mean of the distribution is shifting to the right, going by $10^{-4}\sqrt{x}$, its width is larger than the average strain. This suggests that, should this scenario be at work, the corresponding distribution of η values would be so broad as to wash out any signal. The standard deviation also increases with concentration approximately as the square root.

For these reasons, it is compelling to look for an alternative explanation to the internal-strain theory. Below, we discuss how the nonzero η may not be related to the local strain, but rather reflects the presence of unusually slow real-space fluctuations. Specifically, it is put forward that the real-space fluctuations may have a tail extending below the NMR frequency. In the next section, the methodology for analyzing this scenario quantitatively is described.

IV. METHODOLOGY

This study uses ^{75}As NMR experimental data of $Ba(Fe_{1-x}Co_x)_2As_2$ from literature and compares it to DFT calculations of the EFG and the magnitude of the Fe magnetic moment M that we have performed. It is well known that DFT calculations of M are too large in comparison to experiment, and this is observed in the results in the next section. This is usually ascribed to spin fluctuations beyond DFT, which is by construction a mean-field theory [27]. The effects of spin fluctuations can be emulated using reduced Stoner theory (RST) [14]. Following the methodology introduced in Ref. [28], this is done by scaling the spin-dependent part of the exchange and correlation functional with a parameter $0 \leqslant t \leqslant 1$, where $t \to 0$ corresponds to strong fluctuations (full suppression of ordered magnetism) and $t = 1$ gives the usual result with no fluctuations. Now, since tuning the t parameter also affects the orbital composition of the occupied Fe states, the EFG at the As site will also be affected. This way, the EFG can be calculated as a function of M. From this function, the experimental η values can then be used to extract corresponding values of M. These extracted values represent the effective Fe moment as seen on the NMR timescale. This is a quantity of interest which exists only because of fluctuations extending to far lower frequencies than previously appreciated. Now, the calculations can be set up in an antiferromagnetic configuration while tuning t in order to capture what we argue to be instantaneously antiferromagnetic snapshots in the paramagnetic phase. This will allow for the computations to be compared to any experimental probe with any timescale in either the antiferromagnetic or paramagnetic phase. In this study, the probe of interest is NMR, and so the described methodology will allow for extracting the Fe magnetic moment on the NMR timescale. Of course, the protocol described here is a rather simplistic way to account for suppression of magnetism by spin fluctuations, but we expect it to be a good estimate. The reasoning for this is fundamentally due to the fact that simulating spin fluctuations directly in DFT is not possible. However, it is possible to emulate the effects of spin fluctuations using the approach described above. RST has become a standard approach in accounting for spin fluctuations in DFT calculations, showing good experimental agreement [14]. A later application of RST was used to successfully reproduce x-ray emission spectroscopy measurements in 122 materials [28].

For completeness, we included all available NMR data from literature that also had reliable corresponding structural data to be used for the DFT calculations. Citations are given in Fig. 3.

DFT calculations were performed using the augmented plane wave plus local orbitals code WIEN2K [31,32] with a generalized gradient approximation for the exchange and correlation functional [33]. Tetragonal structural data for $x = 0, 0.02, 0.045$ were input but used an antiferromagnetic stripelike configuration with spin polarization turned on while varying t to simulate the effects of spin fluctuations. Similarly, orthorhombic structural data at $x = 0$ were used for comparison to the antiferromagnetic measurements. In cases with $x > 0$ charge doping is modeled by virtual crystal approximation. Also, spin-orbit coupling is not considered in these calculations since it only weakly affects charge density in Fe-pnictides. All DFT calculations were run to self-consistency. Convergence of the EFG was achieved with the default `R-MT*K-MAX` $= 7.00$, `GMAX` $= 12.0$. A **k**-point mesh of $20 \times 20 \times 18$ was necessary to ensure reasonable convergence of η in the low-M limit since at small moments the reduced Stoner procedure tends to be less stable.

V. RESULTS AND DISCUSSION

The computed η vs M results are shown in Fig. 3 with experimental data for comparison. The DFT calculations were run using experimental lattice parameters determined from temperatures in the paramagnetic phase as close to the transition as the data provide since the interesting effects of real-space fluctuations are strongest near the tetragonal-orthorhombic transition. As M is scaled down, a change in η is observed since both the magnetic order and electronic order are tied together. Hence, the horizontal axes can be viewed as the strength of spin fluctuations. The data point for the largest M corresponds to the equilibrium state, that is, no fluctuations. And smaller M corresponds to scenarios where spin fluctuations are strongest. It is clear from the inset of Fig. 3(b) that the equilibrium M value is vastly larger than the experimental measurements of M in the orthorhombic state, which was determined at 5 K [29]. It is believed that, even at absolute zero, quantum fluctuations will suppress M [27].

Since the definition of η for the purposes of this paper deviates from the standard NMR convention of keeping the largest EFG component in the denominator, η can take on any real value, as shown in Fig. 3. In contrast, η defined in the conventional way is shown in Fig. 4(b), and is, by definition, restricted as $0 \leqslant \eta \leqslant 1$. However, this definition of η is not physically meaningful and, hence, is not compared to experimental data. The singularity in Fig. 3(a), near $M = 1.75\ \mu_B$, appears because of the unconventional definition of η and the fact that the signs of V_{aa} and V_{bb} are opposite to each other in that regime. This behavior can be seen in Fig. 4(a) where the EFG components are shown explicitly, and is similar to that observed experimentally in LaFeAsO [34].

In Fig. 3, a clear quadratic behavior of η is found for small values of M, and, as expected, tends to 0 as the magnetic order disappears, and, therefore, the electronic charge density becomes symmetric. Due to real-space fluctuations, the observed magnetic moment depends on the timescale of the probe and, as long as the timescale of the fluctuations is slower than the timescale of the probe, can be nonzero even for measurements performed in the paramagnetic phase. Hence, M determined from different probes can be used to determine the amplitude of the real-space fluctuations. Using the DFT fits and experimental η values, shown in Fig. 3, an effective magnetic moment, as probed by NMR, can be extracted. These values are shown in Fig. 3(b) by the intersecting dashed lines. These extracted moments, compared to moments determined by other experimental probes, are shown in Fig. 5, where a clear difference between the different probes can be seen.

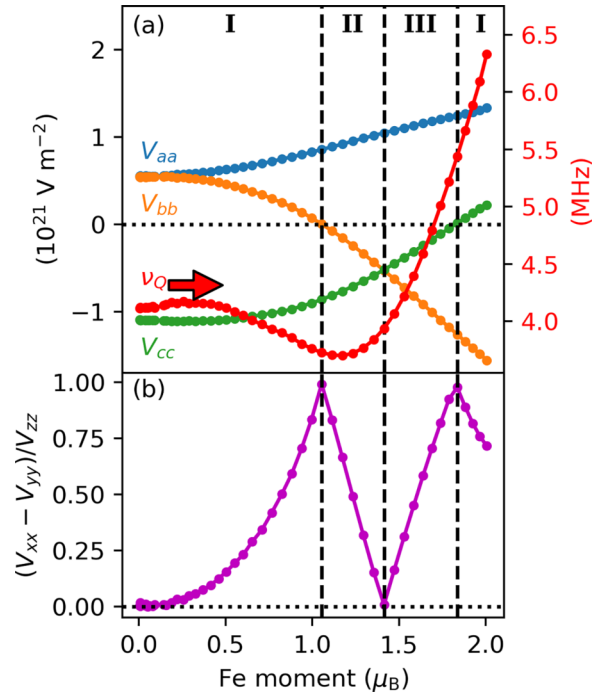

FIG. 4. (a) The components of the computed EFG tensor are plotted on the left axis and the NQR frequency ν_Q, which is proportional to the square root of the EFG components added in quadrature [see Eq. (4)] plotted on the right axis. (b) The EFG asymmetry parameter in the particular principal axes frame such that $|V_{zz}| \geqslant |V_{yy}| \geqslant |V_{xx}|$. In this frame, it is not necessarily the case that $(x, y, z) = (a, b, c)$. A single Co concentration, 2%, was chosen for these plots to illustrate the general behavior of the EFG. Three regimes are identified: (I) $V_{cc} > V_{aa} - V_{bb}$, (II) $V_{aa} > V_{bb} - V_{cc}$, (III) $V_{aa} > V_{cc} - V_{bb}$. This shows how the principal axes frame can change for different values of the Fe magnetic moment and how this conventional choice for the principal axes frame is less desirable than that chosen for Fig. 3.

It is worth noting that typical probes sensitive to spin fluctuations, as, for instance, neutron scattering, measure both spin-space and real-space fluctuations (Fig. 1), and the characteristic large frequency is driven by the former. The NMR asymmetry studied here, on the contrary, is only affected by the latter. Not only are real-space fluctuations much slower, they can also couple with the lattice, which can cause additional dramatic reduction of the frequency scale, as discussed in Ref. [35], where it was argued that the slowdown can extend even to a 100-Hz range [36].

Thus, the experimental results of Ref. [10] can be quantitatively reproduced if one adapts the proposed scenario with a slow tail of real-space fluctuations, and assumes that the fluctuations reduce the effective magnetic moment by about

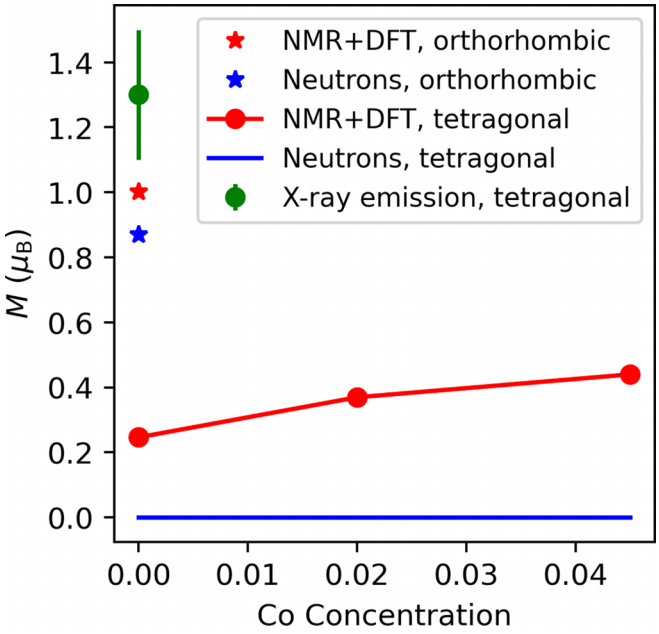

FIG. 5. Comparison of the extracted magnetic moments from Fig. 3, corresponding to the intersection of the experimental NMR η values with the DFT fits (labeled as "NMR + DFT" in the plot) with magnetic moments determined by neutron scattering and x-ray emission spectroscopy (XES). Since neutron scattering has a longer timescale compared to that of NMR, the measured neutron diffraction magnetic moments [29] will be averaged out to a greater degree due to real-space fluctuations and thus are consistently smaller than the NMR + DFT moments. In contrast, the timescale of x-ray emission spectroscopy [37] is effectively instantaneous and therefore shows a moment larger than both NMR + DFT and neutron scattering.

one order of magnitude compared to its DFT value. Recall that we only include a reduction due to real-space fluctuations, otherwise, the magnetic moments within the NMR timescale would have definitely averaged to zero.

One question remains: What in that case would be the origin of a Curie-Weiss temperature dependence found in Ref. [10]? To answer this question, we assume that the spectral density of the real-space fluctuations can be described by the classical Ornstein-Zernicke formula:

$$\langle M^2 \rangle \propto \int_0^{\nu_{\mathrm{NMR}}} \frac{1}{\pi} \frac{\gamma}{\gamma^2 + \nu^2} \, d\nu = \frac{1}{\pi} \arctan \frac{\nu_{\mathrm{NMR}}}{\gamma}, \qquad (6)$$

where $\langle M^2 \rangle$ is the mean-square amplitude of the magnetic moment fluctuating slower than ν_{NMR}. It is important to note that the γ defined here is for the real-space fluctuations only, and should not be confused with γ determined by neutron scattering, which is large and on the order of millivolts [38], and primarily determined by spin-space fluctuations. Still, $\nu_{\mathrm{NMR}} \ll \gamma$, so, to first order, this expression is proportional to $\nu_{\mathrm{NMR}}/\gamma$. Now, if one assumes that γ naturally depends on temperature linearly, and using the fact that η depends on M quadratically for small M, $\eta = AM^2$, and taking $\gamma = \alpha + \beta T$, we have

$$\eta = \frac{A\nu_{\mathrm{NMR}}}{\alpha + \beta T}, \qquad (7)$$

which has the same functional form as the Curie-Weiss law.

VI. CONCLUSIONS

We presented DFT calculations of the Fe magnetic moment and EFG asymmetry parameter to investigate the peculiar observation of a nonzero asymmetry in the paramagnetic phase. While the original authors of that observation favored an interpretation in terms of impurities and imperfections in the crystal as a source of internal strain inducing asymmetry, we introduced an alternative explanation focused on spin dynamics as the culprit. In particular, we proposed that there exist anomalously slow real-space fluctuations of the Fe magnetic moments even in the formally paramagnetic phase, which break the C_4 symmetry that is normally expected to exist in that phase. It was shown in Eq. (7) how the Ornstein-Zernicke formula in conjunction with the quadratic behavior of η with respect to the Fe magnetic moment can reproduce the functional form of the Curie-Weiss law in the appropriate limits. While the results of this study only covered a single material, we believe that this methodology can be extended to more materials in the 122 family and as well as the 111 family. It is generally believed that superconductivity that develops in the paramagnetic phase arises from Fermi-surface geometries characteristic of the nonmagnetic electronic structure. Therefore, if the proposed mechanism of the effect described in this paper is confirmed in general, revisiting the theory of superconductivity in FeSCs may be in place.

ACKNOWLEDGMENTS

This work was supported by the National Science Foundation (Awards No. 1711118 and No. 2214194), the Quantum Science and Engineering Center at George Mason University, and through resources provided by the Office of Research Computing at George Mason University funded in part by grants from the National Science Foundation (Awards No. 1625039 and No. 2018631). We would also like to acknowledge N. Curro and R. Fernandes for insightful conversations.

[1] P. J. Hirschfeld, M. M. Korshunov, and I. I. Mazin, Rep. Prog. Phys. **74**, 124508 (2011).
[2] A. Chubukov, Annu. Rev. Condens. Matter Phys. **3**, 57 (2012).
[3] R. M. Fernandes, A. V. Chubukov, and J. Schmalian, Nat. Phys. **10**, 97 (2014).
[4] E. Bascones, B. Valenzuela, and M. J. Calderón, C. R. Phys. **17**, 36 (2016).
[5] N. D. Mermin and H. Wagner, Phys. Rev. Lett. **17**, 1133 (1966).
[6] I. Mazin and J. Schmalian, Phyisca C **469**, 614 (2009).
[7] K. Kitagawa, N. Katayama, K. Ohgushi, M. Yoshida, and M. Takigawa, J. Phys. Soc. Jpn. **77**, 114709 (2008).
[8] J. M. Ok, S.-H. Baek, C. Hoch, R. K. Kremer, S. Y. Park, S. Ji, B. Büchner, J.-H. Park, S. I. Hyun, J. H. Shim, Y. Bang, E. G. Moon, I. I. Mazin, and J. S. Kim, Nat. Commun. **8**, 2167 (2017).
[9] N. Mannella, J. Phys.: Condens. Matter **26**, 473202 (2014).

[10] M. Toyoda, A. Ichikawa, Y. Kobayashi, M. Sato, and M. Itoh, Phys. Rev. B **97**, 174507 (2018).
[11] M. Toyoda, Y. Kobayashi, and M. Itoh, Phys. Rev. B **97**, 094515 (2018).
[12] R. G. Bryant, J. Chem. Educ. **60**, 933 (1983).
[13] Y. Yao, R. Willa, T. Lacmann *et al.*, Nat. Commun. **13**, 4535 (2022).
[14] L. Ortenzi, I. I. Mazin, P. Blaha, and L. Boeri, Phys. Rev. B **86**, 064437 (2012).
[15] C. P. Slichter, *Principles of Magnetic Resonance* (Springer, Berlin, 1990).
[16] G. Muha, J. Magn. Res. **53**, 85 (1983).
[17] A. Abragam, *The Principles of Nuclear Magnetism* (Oxford University Press, Oxford, 1961).
[18] B. H. Suits, in *Handbook of Applied Solid State Spectroscopy*, edited by D. R. Vij (Springer, Boston, MA, 2006), pp. 65–96.
[19] H.-J. Grafe, D. Paar, G. Lang, N. J. Curro, G. Behr, J. Werner, J. Hamann-Borrero, C. Hess, N. Leps, R. Klingeler, and B. Büchner, Phys. Rev. Lett. **101**, 047003 (2008).
[20] H. Mukuda, N. Terasaki, H. Kinouchi, M. Yashima, Y. Kitaoka, S. Suzuki, S. Miyasaka, S. Tajima, K. Miyazawa, P. Shirage, H. Kito, H. Eisaki, and A. Iyo, J. Phys. Soc. Jpn. **77**, 093704 (2008).
[21] H. Fukazawa, T. Yamazaki, K. Kondo, Y. Kohori, N. Takeshita, P. M. Shirage, K. Kihou, K. Miyazawa, H. Kito, H. Eisaki, and A. Iyo, J. Phys. Soc. Jpn. **78**, 033704 (2009).
[22] R. Zhou, L. Y. Xing, X. C. Wang, C. Q. Jin, and G.-q. Zheng, Phys. Rev. B **93**, 060502(R) (2016).
[23] K. Kitagawa, N. Katayama, K. Ohgushi, and M. Takigawa, J. Phys. Soc. Jpn. **78**, 063706 (2009).
[24] T. Kissikov, R. Sarkar, M. Lawson, B. T. Bush, E. I. Timmons, M. A. Tanatar, R. Prozorov, S. L. Bud'ko, P. C. Canfield, R. M. Fernandes, W. F. Goh, W. E. Pickett, and N. J. Curro, Phys. Rev. B **96**, 241108(R) (2017).
[25] L. D. Landau and E. M. Lifshitz, *Theory of Elasticity* (Pergamon Press, London, 1959).
[26] K. Burns, A. M. Z. Tan, H. Gordon, T. Wang, A. Gabriel, L. Shao, R. G. Hennig, and A. Aitkaliyeva, Phys. Rev. B **102**, 085421 (2020).
[27] I. I. Mazin, M. D. Johannes, L. Boeri, K. Koepernik, and D. J. Singh, Phys. Rev. B **78**, 085104 (2008).
[28] L. Ortenzi, H. Gretarsson, S. Kasahara, Y. Matsuda, T. Shibauchi, K. D. Finkelstein, W. Wu, S. R. Julian, Y.-J. Kim, I. I. Mazin, and L. Boeri, Phys. Rev. Lett. **114**, 047001 (2015).
[29] Q. Huang, Y. Qiu, W. Bao, M. A. Green, J. W. Lynn, Y. C. Gasparovic, T. Wu, G. Wu, and X. H. Chen, Phys. Rev. Lett. **101**, 257003 (2008).
[30] N. Ni, M. E. Tillman, J.-Q. Yan, A. Kracher, S. T. Hannahs, S. L. Bud'ko, and P. C. Canfield, Phys. Rev. B **78**, 214515 (2008).
[31] P. Blaha, K. Schwarz, G. K. H. Madsen, D. Kvasnicka, J. Luitz, R. Laskowski, F. Tran, and L. D. Marks, *WIEN2k, An Augmented Plane Wave + Local Orbitals Program for Calculating Crystal Properties* (Karlheinz Schwarz, Techn. Universität Wien, Austria, 2018).
[32] P. Blaha, K. Schwarz, F. Tran, R. Laskowski, G. K. H. Madsen, and L. D. Marks, J. Chem. Phys. **152**, 074101 (2020).
[33] J. P. Perdew, K. Burke, and M. Ernzerhof, Phys. Rev. Lett. **77**, 3865 (1996).
[34] H.-J. Grafe, P. Lepucki, M. Witschel, A. P. Dioguardi, R. Kappenberger, S. Aswartham, S. Wurmehl, and B. Büchner, Phys. Rev. B **101**, 054519 (2020).
[35] G. Drachuck, M. Schütt, A. E. Böhmer, P. P. Orth, A. Kreyssig, R. Prozorov, S. L. Bud'ko, R. M. Fernandes, and P. C. Canfield, arXiv:1708.02156.
[36] Reference [35] was withdrawn because issues were discovered in the experimental data; however, the validity of the theoretical arguments, to our best knowledge, has not been questioned.
[37] H. Gretarsson, A. Lupascu, J. Kim, D. Casa, T. Gog, W. Wu, S. R. Julian, Z. J. Xu, J. S. Wen, G. D. Gu, R. H. Yuan, Z. G. Chen, N.-L. Wang, S. Khim, K. H. Kim, M. Ishikado, I. Jarrige, S. Shamoto, J.-H. Chu, I. R. Fisher *et al.*, Phys. Rev. B **84**, 100509(R) (2011).
[38] L. W. Harriger, M. Liu, H. Luo, R. A. Ewings, C. D. Frost, T. G. Perring, and P. Dai, Phys. Rev. B **86**, 140403(R) (2012).